Section 5

Development of and studies with regional and smaller-scale atmospheric models, regional ensemble, monthly and seasonal forecasting

Improved assimilation of SEVIRI radiances over land in meso-scale models using Land Surface Temperature retrievals.

Guedj Stephanie, Fatima Karbou, Florence Rabier
CNRM-GAME/Meteo-France and CNRS

Infra-red satellite data gathered from the SEVIRI[1](Schmetz et al., 2002) radiometer, which is onboard the geostationary satellite MSG, are operationally assimilated in the AROME[2] and ALADIN[3] limited area models (Montmerle et al., 2007). Measurements come from 12 spectral channels with an unprecedented spatio-temporal resolution (1 image every 15 minutes with a 3km horizontal resolution). These measurements bring useful information about the state of the atmosphere (temperature and humidity) over several layers and of the surface.

Nowadays, SEVIRI observations that are sensitive to atmospheric low-levels are rejected over land partly because of an inappropriate description of the Land Surface Temperature (LST) and of the Land Surface Emissivity (LSE) in the model. Out of the constraints of data assimilation, many studies were carried out to improve our understanding of the LST (Qin et al., 2001; Sobrino et al., 2004 …) and the LSE (Trigo et al., 2008; Borbas and Ruston., 2010) variability.

The potential reduction of these uncertainties which presently restrict the assimilation of surface-sensitive channels over land has been evaluated (1) when the LST is deduced from SEVIRI window channels using a single-channel method and (2) when the LSE atlases produced by the EUMETSAT LSA-SAF[4] replace the static default value of 0.98 used in the radiative tranfer model RTTOV.

First, retrieved LST (called LST-SEV hereafter) were evaluated against independent observations/products: LST-MODIS[5], LST-Land-SAF, T2M (2 m temperature), LST-ALADIN which is the land surface temperature analysed by the ALADIN model. Some differences due to instrumental specifications were found between LST-MODIS and LST-SAF. The LST-SEV and LST-SAF products were found in good agreement over Europe. Cold (warm) biases were observed during day-time (night-time) when comparing LST-SEV, retrieved from channels IR8.7 and IR10.8, with LST-ALADIN which seems to be due to an under-estimation of the diurnal cycle in the model. Then, an emissivity atlas has been combined with these different LST-SEV to simulate SEVIRI brightness temperatures. The simulations were compared to SEVIRI observations. The comparison shows that SEVIRI channel IR10.8 is the most suitable one for LST retrieval (Guedj et al., 2011).

These developments were then tested in a data assimilation context, thus enabling to use more SEVIRI data over land. Two assimilation experiments were run over a 3-month period during summer 2009, one of which is representative of the operational model (CTL) while the other differs by the assimilation of more SEVIRI data over land through a better representation of the emissivity and surface temperature (EXP). We show that the forecast impact is generally neutral to positive over Europe with some positive impact over Southern Europe. SEVIRI data also improve the quality of analyses, particularly those of Total Column Water Vapour (TCWV, see figure 1), and this is substantiated through comparisons with independent GPS measurements (figures 2), (Guedj et al., 2012). These developments should be implemented soon in operations version.

[1] Spinning Enhanced Visible and Infrared Imager
[2] Application de la Recherche à l'Opérationnel à Méso-Echelle
[3] Aire Limitée Adaptation Dynamique Initialisation, développement International
[4] European Organisation for the Exploitation of Meteorological Satellites - Land Surface Analysis - Satellite Application Facility
[5] MODerate resolution Imaging Spectroradiometer

Figure 1: Mean analysis difference in TCWV between EXP (with SEVIRI over land) and CTL (without SEVIRI over land) at 12UTC. TCWV maps are averaged over 45 days (1 September - 5 October 2009). Red (blue) colours means that EXP contribute to decrease (increase) moisture in the analysis as regard to the CTL.

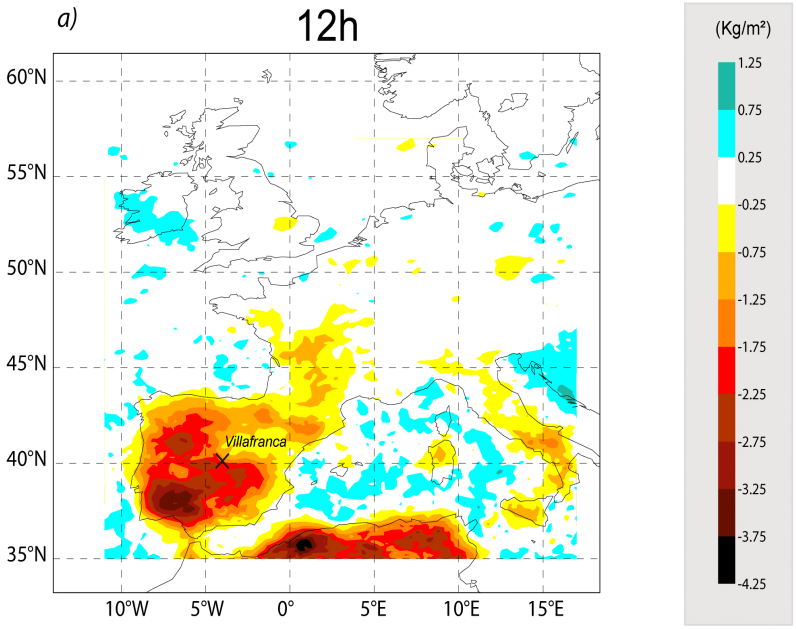

Figure 2: Average values of TCWV from GPS (Villafranca)(dotted black line), EXP (black thin line) and CTL (grey line) according to the assimilation cycle (0-6-12-18 UTC).TCWV values are averaged over 45 days (September 1 to October 15 of 2009)

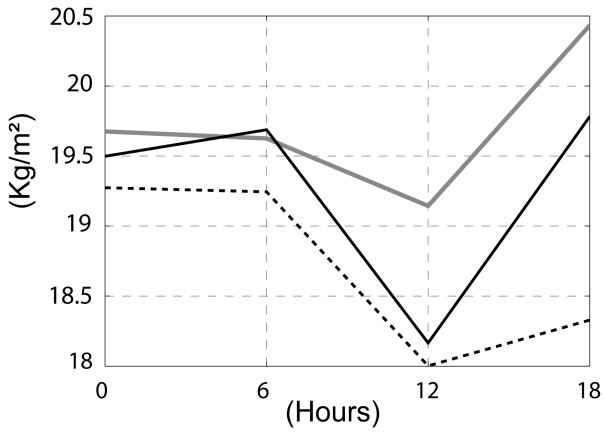

References

Borbas, E. and Ruston, B. (2010). "The RTTOV UWiremis IR land surface emissivity module". NWPSAF Tech. Memo. AS09-04.

Guedj, S., Karbou, F., and Rabier, F. (2011). Land Surface Temperature estimation to improve the assimilation of SEVIRI radiances over land. *JGR*, 116(D14107) :18 pp.

Guedj, S., Karbou, F., Rabier, F., Guidard, V., and Montmerle, T. (2012), Improved assimilation of observations from SEVIRI over land. *MWR*. Submitted.

Montmerle, T., Rabier, F., and Fisher, C. (2007). Relative impact of polar-orbiting and geostationary satellite radiances in the Aladin/France numerical weather prediction system. *QJRMS*,133.

Qin, Z., Karnieli, A., and Berliner, P. (2001). A mono-window algorithm for retrieving land surface temperature from landsat tm data and its application to the Israel-Egypt border region. *IJRS*, 22(18) :3719–3746.

Schmetz, J., Pili, P., Tjemkes, S., Just, D., Kerkmann, J., Rota, S., and Ratier, A. (2002). An Introduction to Meteosat Second Generation (MSG). *BAMS*, 83.

Sobrino, J., Jimenez-Munoz, J., El-Kharraz, J., Gomez, M., Romaguera, M., and Soria, G. (2004). "Single-channel and two-channel methods for land surface temperature retrieval from DAIS data and its application to the Barrax site". *IJRS*, 25(1) :215–230.

Trigo, I., Peres, L., DaCamara, C., and Freitas, S. (2008). Thermal land surface emissivity retrieved from SEVIRI/Meteosat. IEEE Transaction on Geoscience and remote sensing, 46(2) :307–315.

Development of the Physics Library and its application to ASUCA

TABITO HARA[1*], KOHEI KAWANO[1], KOHEI ARANAMI[1], YUJI KITAMURA[2],
MASAMI SAKAMOTO[1], HIROSHI KUSABIRAKI[1], CHIASHI MUROI[1] AND JUNICHI ISHIDA[1]
[1]*Numerical Prediction Division, Japan Meteorological Agency,* [2]*Meteorological Research Institute*
1-3-4, Ote-machi, Chiyoda-ku, Tokyo 100-8122, Japan

1 Introduction

Achieving efficient operations of numerical models on scalar multi-core architecture is a challenging issue in light of the rapid expansion of the market share for massive scalar computers in the supercomputer world. In order to overcome the problems anticipated in this regard, we have been developing a new nonhydrostatic dynamical core named ASUCA (Ishida et al. 2009, 2010). Flux-form fully compressible governing equations are adopted and discretized using the finite volume method to secure mass conservation. The flux limiter function proposed by Koren (1993) is employed to satisfy monotonicity and avoid numerical oscillations. The third-order Runge-Kutta scheme is adopted for the time integration of the system. A study by Ishida et al. (2010) involving a number of idealized experiments for dynamics showed that ASUCA exhibits high levels of performance. It has also been confirmed that mass conservation in the domain is well satisfied.

In order to utilize the new model as a practical forecast model, it is essential to implement physical processes. Although simply porting the physical processes of the current operational nonhydrostatc mesoscale model (JMA-NHM, Saito et al. 2007) may seem the easiest way to achieve this, maintaining and developing both codes would involve a huge cost burden. The Physics Library, currently under development, represents a trial effort to realize the sharing code for physical processes not only between ASUCA and JMA-NHM but also among various other models. The initiative is expected to facilitate efficient development of physical processes and promote related collaboration.

This paper describes the basic design of the Physics Library and outlines its purposes and current specifications. ASUCA is the first model for the library to be installed into practical models. Preliminary results of ASUCA with physical processes are also discussed here.

2 Physics Library

Computer libraries generally contain collections of subroutines and functions commonly used by various applications. Likewise, the Physics Library is intending to serve as a repository for various subroutines related to physical processes with unified coding and interface rules, and allows them to be shared among various forecast models. Physical processes in the library are implemented as vertical one-dimensional models aiming at low memory usage to improve cache efficiency, which is absolutely crucial for scalar computers. This simple one dimensional implementation is expected to make the development of physical processes more efficient.

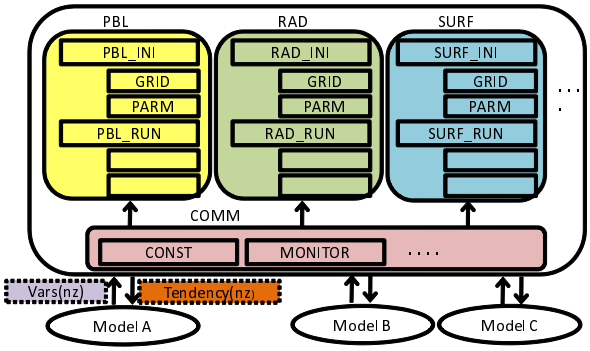

Fig. 1: A schematic representation of the Physics Library and its various components (`COMM`, `PBL`, `RAD`, `SURF` etc). Each component is basically independent and can contain one or more schemes. The library receives inputs (`Vars(nz)`) from models and returns tendencies (`Tendency(nz)`) to them.

The fundamental role of physical processes is to evaluate temporal tendency of prognostic variables brought by subgrid transport related to convection, turbulence and gravity waves as well as other effects that the governing equations of dynamics cannot describe (radiation, condensation, etc.). In consideration of the role played by physical processes, the library returns tendencies of prognostic variables without changing the variables themselves and other inputs provided by users. When users pass one dimensional arrays of physical quantities to the library, they can receive tendencies of prognostic variables, as shown in Fig. 1.

A number of idealized test programs following the configurations of international intercomparison projects for physical processes (GABLS2, GABLS3, EUROCS, GCSS-ARM, TRMM-LBA, etc.) are also included in the package of the library. With the test programs, one can evaluate performance of physical processes and compare two or more schemes contained in the library each other. The programs can also be referred to as sample code to show how each subroutine in the library is used. The test programs are expected to help users develop and evaluate physical processes and to facilitate the installation of subroutines contained in the library to practical models.

Documentation on the interfaces of subroutines in the library are quite important to show the usage of the library. However, interface modification is often not accompanied by documentation updates especially if the documents and code are separated. To secure simultaneous updating, documentation on the interfaces is included with code in the form of special

*E-mail: `tabito.hara@met.kishou.go.jp`

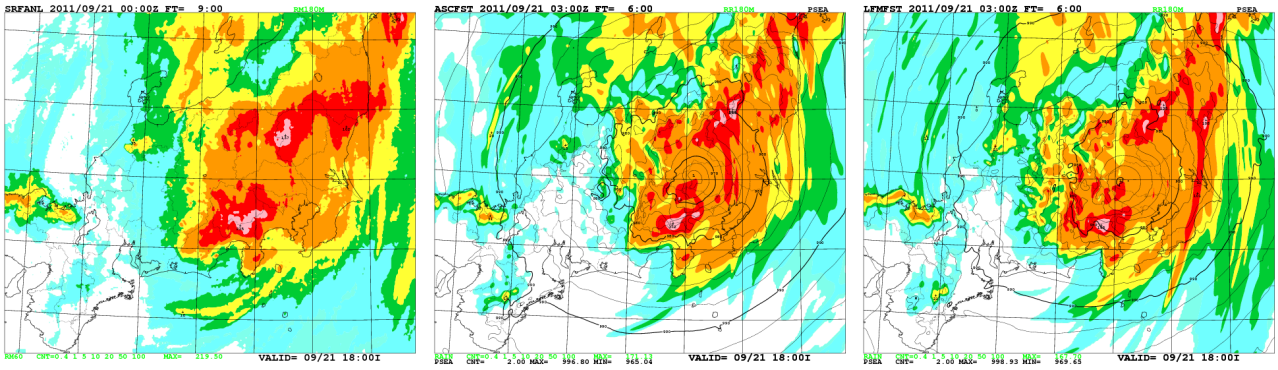

Fig. 2: Simulation results initialized for 03 UTC on 21 September, 2011. MSLP and 3-hour accumulated precipitation at 6 hours from the initial time are displayed with the corresponding precipitation observations. Left: observation (precipitation only), center: ASUCA, right: JMA-NHM.

comment lines. A tool can be used to extract this inline information and convert it to useful formats such as HTML and LaTeX.

Currently, physical schemes implemented in JMA-NHM have been just ported into the library. We are going to collect more schemes from mesoscale weather forecast models to global climate models to make it a true library resource. Intercomparison of schemes is one of the basic developments of physical processes, and will be facilitated by the library once it is populated with various schemes.

Although the library was originally intended to support the sharing of code for physical processes, it also supports the more efficient development of physical processes which requires detailed and extensive knowledge of physics and meteorology. The resource also serves as a basis of "seamless" model development of which importance is often claimed recently.

3 Application of "Physics Library" to ASUCA

Once most physical processes equivalent to those of the current operational mesoscale model were implemented in the Physics Library, attempts were made to install physical processes using it. It took just a week for a developer of ASUCA (who is not a developer of the library) to implement boundary layer, radiation, surface and microphysics onto ASUCA referring to the documentation on interfaces of the library. To check correct implementation, configurations identical to those of the idealized experiments included as sample and test environments in the library were also built in ASUCA. It has been confirmed that ASUCA with the physical processes produced results almost identical to those of the library's test environment, indicating that the physical processes were successfully installed as the developer of the library intended. The simple, organized, and documented interfaces of the library are expected to help model developers implement and try various physics schemes.

4 An example of the simulation of ASUCA with physical processes

The successful installation of physical processes using the Physics Library as described above allows comparison between ASUCA and other practical models including the current operational model (JMA-NHM). Figure 2 shows an example of such comparison with reference to the corresponding observation. In this case, it can be seen that both models produce good forecasts with results similar to those of actual observation.

5 Conclusion and future plans

ASUCA can now be compared with other practical models because physical processes have been implemented as appropriate. From the early stages of development of ASUCA, we consider that sharing code of physical processes among models as the Physics Library is essential for efficient progress.

As far as the preliminary evaluation, ASUCA with physical processes produces results similar to those of the current operational mesoscale model JMA-NHM in regards to the distribution of precipitation brought by a typhoon. Further evaluation of ASUCA is now being carried out to allow comparison of its statistical aspects to those of JMA-NHM.

The successful use of the Physics Library with ASUCA represents its first application to practical models. To cement its status as a fundamental tool supporting development and collaboration related to physical processes, it is necessary to collect more schemes and implement more test cases.

References

Ishida, J., C. Muroi, and Y. Aikawa, 2009: Development of a new dynamical core for the nonhydrostatic model. *CAS/JSC WGNE Res. Activ. Atmos. Oceanic Modell.*, **39**, 0509–0510.

Ishida, J., C. Muroi, K. Kawano, and Y. Kitamura, 2010: Development of a new nonhydrostatic model ASUCA at JMA. *CAS/JSC WGNE Res. Activ. Atmos. Oceanic Modell.*, **40**, 0511–0512.

Koren, B., 1993: A Robust Upwind Discretization Method for Advection, Diffusion and Source Terms. *CWI Report*, NM–R9308.

Saito, K., J. Ishida, K. Aranami, T. Hara, T. Segawa, M. Narita, and Y. Honda, 2007: Nonhydrostatic Atmospheric Models and Operational Development at JMA. *J. Meteor. Soc. Japan*, **85B**, 271–304.

Testing a multi-model approach for providing boundary conditions to a regional ensemble.

Chiara Marsigli, Andrea Montani, Tiziana Paccangnella

ARPA-SIMC (HydroMeteoClimate Service of Emilia-Romagna), Bologna, Italy
E-mail: *cmarsigli@arpa.emr.it*

Aiming at the development of an ensemble forecasting system for the short-range, the COSMO Consortium has chosen to explore the validity of a multi-analysis multi-model (MAMM) approach for providing initial and boundary condition perturbation to an ensemble based on the COSMO Limited-area model.

This approach has been implemented in the experimental COSMO-SREPS ensemble (COSMO Short-Range Ensemble Prediction System, Marsigli et al., 2009), which receives initial and boundary conditions by few state-of-the art operational deterministic runs (the IFS model of ECMWF, the GME model of DWD, the GFS model of NCEP). The performance of COSMO-SREPS is compared against COSMO-LEPS (Montani et al., 2011), the operational regional ensemble of the COSMO Consortium, which receives initial and boundary condition perturbations from some members of the global ensemble of ECMWF. Both systems are made up by 16 integrations of the COSMO model with 7 km horizontal mesh-size and they both benefit also of perturbations of the COSMO model physics parameters. Two different combinations of COSMO-LEPS and COSMO-SREPS have also been evaluated: a 20-member ensemble made up of the 16 COSMO-LEPS runs plus 4 COSMO-SREPS runs (mix20) and a 16-member ensemble made up by the first 12 COSMO-LEPS runs plus 4 COSMO-SREPS runs (mix16). The 4 COSMO-SREPS runs selected are nested on the 3 different global models, plus a control member.

Verification is performed in terms of Probabilistic Quantitative Precipitation Forecast (PQPF), using a dense raingauge network covering northern Italy. The verification period is winter 2010/2011.

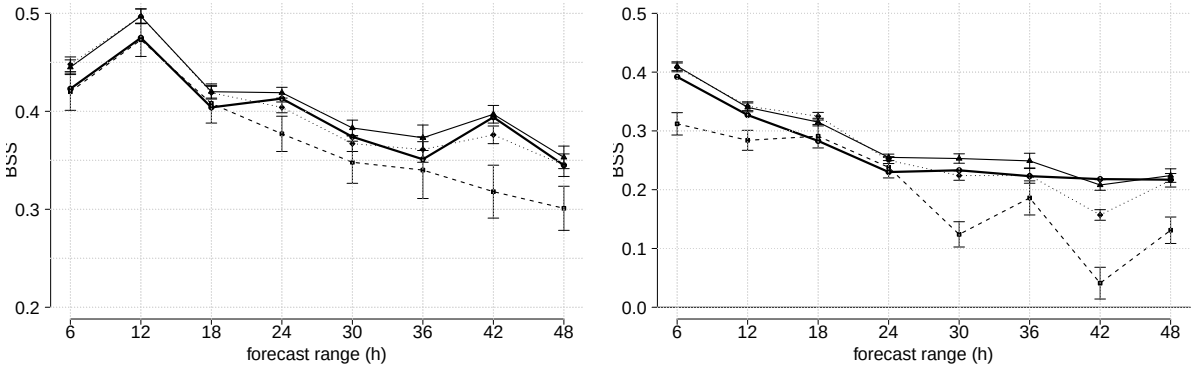

Figure 1: Brier Skill Score as a function of the forecast range for the event "mean of the precipitation exceeding 1mm/6h" (left) and "5mm/6h" (right). The solid thick line is for COSMO-LEPS, the dashed line is for COSMO-SREPS, the dotted line for mix16 and the solid thin line for mix20.

In Figure 1, the Brier Skill Score is plotted as a function of the forecast range. The average of the precipitation values on the grid points falling in each box of 0.5 x 0.5 degrees covering the verification area is compared against the average of the observed values falling in the same box, for all the boxes and for the whole period.

COSMO-LEPS performs better than COSMO-SREPS for almost all the forecast ranges, the difference between the two ensembles being more pronounced for the 5mm/6h threshold. The error bars are

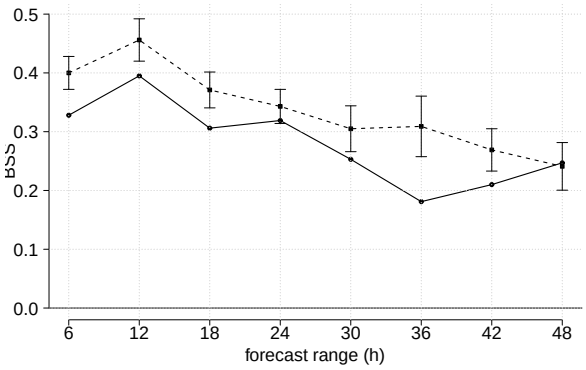

Figure 2: Brier Skill Score a function of the forecast range for the event "mean of the precipitation exceeding 1mm/6h" for the 3-member COSMO-LEPS (solid line) and COSMO-SREPS (dashed line).

obtained with an hypothesis testing, at 95% of confidence, that the score differs from the COSMO-LEPS one. Mix16 performs better than COSMO-LEPS for the first 18-24 h, while mix20 performs better than COSMO-LEPS for almost the whole forecast range, especially for the higher precipitation threshold. Therefore, keeping the ensemble size fix, to drive some COSMO members with the MAMM system, instead of with few more members of the EPS, brings some benefit, but only in the first 24 h. A longer-lasting skill increase could be obtained by adding the 4 MAMM-driven members to the already existing COSMO-LEPS.

The unsatisfactory performance of the MAMM approach for boundaries is probably due to the few models available for providing perturbations to COSMO-SREPS, with respect to the somehow large (16 members) ensemble size. Then, the relation between the number of different initial and oundary conditions perturbations and the ensemble size is addressed, by computing the scores relative to the 3-member versions of the two ensembles (Figure 2). The 3-member COSMO-LEPS is made up by the first 3 members, while the 3-member COSMO-SREPS is made up by members driven by the 3 different global runs. The 3-member COSMO-SREPS perfoms better than the 3-member COSMO-LEPS, within the 95% confidence level. This result stresses the importance of the availability of as many as possible global model runs to provide boundary conditions to a LAM ensemble. On the other hand, it indicates that, when only a small size LAM ensemble is feasible, the multi-model approach for boundaries gives better results.

On the basis of these results, an hybrid approach will be tested, where the 16 COSMO-LEPS runs are merged with some COSMO-SREPS. The performance of the hybrid system and its affordability will be subject to further studies.

REFERENCES

Marsigli, C., 2009: COSMO-SREPS Priority Project "Short Range Ensemble Prediction System (SREPS): final report. COSMO Technical Report No. 13, available at http://www.cosmo-model.org/public/techReports.htm

Montani, A., Cesari, D., Marsigli, C. and Paccagnella, T., 2011: Seven years of activity in the field of mesoscale ensemble forecasting by the COSMO-LEPS system: main achievements and open challenges. *Tellus*, **63A**, 605-624.

Impact of soil-moisture initialisation on the quality of short-range COSMO-LEPS forecasts

Andrea Montani, C. Marsigli and T. Paccagnella

ARPA–SIMC (HydroMeteoClimate Service of Emilia-Romagna), Bologna, Italy
E-mail: amontani@arpa.emr.it

Introduction

In the framework of limited–area ensemble forecasting, the COSMO–LEPS system was the first mesoscale ensemble application running on a daily basis in Europe since November 2002 (Montani et al., 2003). In the following years, several upgrades were made with a positive impact on COSMO–LEPS forecast skill of precipitation in the short and early medium–range (Montani et al., 2011). As a further amelioration of the system, it was decided to test different approaches to initialise the soil fields of COSMO–LEPS ensemble members (mainly temperature and soil water–content). It was studied the impact of the different initialisations on the quality of short-range forecasts provided by the system during winter and spring 2011. In this work, the attention is focused on the forecast skill of 2-metre temperature and 2-metre dew-point temperature (T2M and TD2M, respectively), which are heavily influenced by the soil properties, for ranges up to 48 hours. From December 2010 up to mid-March 2011, the following experimentation was undertaken: in addition to the operational ensemble (referred to as "ope") where the lower boundary conditions are interpolated from ECMWF EPS members, it was run in parallel a further 16–member ensemble (referred to as "test"), where the soil fields were provided by COSMO-EU, the deterministic model integration operationally run at the German Weather Service. The COSMO-EU fields passed to COSMO-LEPS members included temperature, water content and ice content of the soil layers, temperature of snow surface, water content of snow and density of snow. These fields were used as lower boundary conditions for all COSMO-LEPS members before the beginning of the model integrations. Like COSMO–LEPS, COSMO–EU runs at 7km and the grids, as well as the properties of the soil, are the same for both systems. Therefore, it is hoped that the provision of lower-boundary conditions at higher resolution and from the same type of model can enhance the description of soil temperature and humidity in COSMO–LEPS members, this having an overall positive impact on the forecast skill of near–surface fields. In the next section, the performance of "ope" and "test" will be assessed, considering the forecast skill of the ensemble mean from fc+0h to fc+48h every 3h.

Methodology and results

As for observations, we used the data obtained from the SYNOP reports available on the Global Telecommunication System (GTS). In order to assess the skill of the system in a comprehensive way, verification was performed over three different domains:

1. "fulldom": about 1400 stations over the entire COSMO-LEPS integration domain;
2. "mapdom": about 410 stations over the area 43N–50N, 2E–18E;
3. "flatdom": the same as "mapdom", but for stations with altitude below 100 m (on average, about 50 stations).

As for the comparison of model forecasts against SYNOP reports, we selected the grid point closest to the observation and we corrected the T2M forecasts according to the difference between

the elevation of the station and the height of the selected grid-point. The verification was performed over a 100–day period, from 1 December 2010 to 15 March 2011 and the following deterministic scores (Wilks, 1995) were computed: the mean-absolute error (MAE) and the bias.

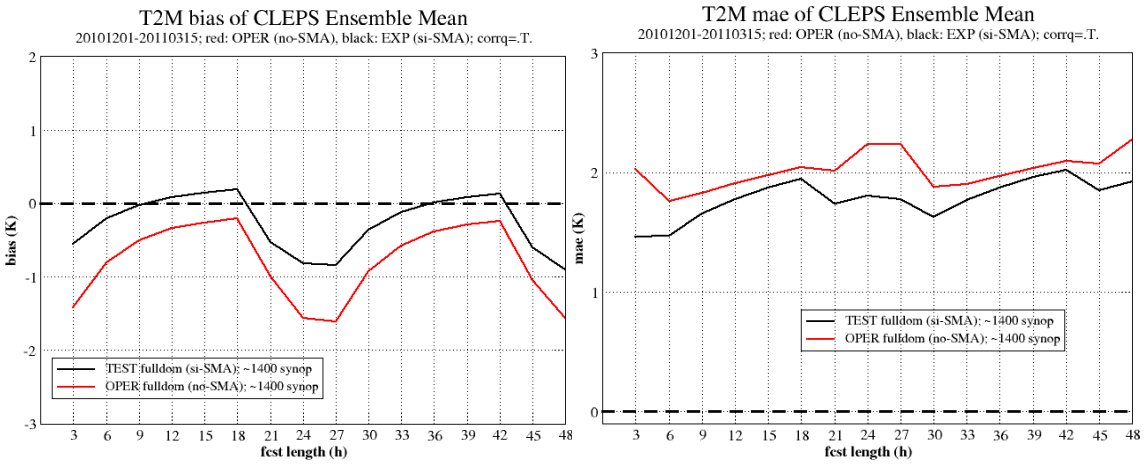

Figure 1: Bias (left panel) and mean–absolute error (right panel) of the 2–metre temperature ensemble mean of "oper" (red) and "test" (black) over the "fulldom" (in Kelvin). Scores are calculated over the period 1 December 2010 - 15 March 2011.

The skill of the two ensembles in terms of T2M over "fulldom" is summarised in Fig. 1, where the bias (left panel) of the ensemble mean is plotted against the forecast range for both "oper" and "test" configurations. It can be noticed that the bias is closer to zero for the "test" ensemble, which takes the soil fields from COSMO-EU. The improvement is systematic for all forecast ranges, contributing to the reduction of the cold bias in COSMO–LEPS integrations. In addition to that, the bias oscillations with forecast range have smaller amplitudes for the "test" ensemble. As for the MAE (right panel of Fig. 1), the better performance of the "test" ensemble is confirmed for all forecast ranges up to 48 hours. The positive impact of using more accurate lower boundary conditions is particularly evident for day–time verification (forecast ranges +24-27h). These results are confirmed when verification is performed over either "mapdom" or "flatdom", where the reduction of the MAE is even more evident for day–time verification. In addition to that, the "test" ensemble outperforms "oper"also in terms of prediction of TD2M over al domains (not shown). Following the indications provided by the above–mentioned scores and thanks to the neutral impact on total precipitation, the new initialisation of soil fields was implemented operationally on 11 April 2011 and has been running on a daily basis since then. As for the future, it is envisaged to continue the systematic verification of the system, to monitor the added value of the new soil initialisation and to study new possible ameliorations.

References

Montani A., Capaldo M., Cesari D., Marsigli C., Modigliani U., Nerozzi F., Paccagnella T., Tibaldi S., 2003. Operational limited–area ensemble forecasts based on the 'Lokal Modell'. ECMWF Newsletter No. 98. Available from: European Centre for Medium–Range Weather Forecasts, Shinfield Park, Reading RG2 9AX, UK.

Montani A., Cesari D., Marsigli C., Paccagnella T., 2011. Seven years of activity in the field of mesoscale ensemble forecasting by the COSMO-LEPS system: main achievements and open challenges. *Tellus*, **63A**, 605–624. DOI: 10.1111/j.1600-0870.2010.00499.x

Wilks, D. S. 1995. Statistical Methods in the Atmospheric Sciences. Academic Press, NY, 467.

Preliminary Results of Mesoscale Ensemble Prediction with Stochastic Parameterization

Kosuke Ono
Numerical Prediction Division, Japan Meteorological Agency, Tokyo, Japan
E-mail: kou.ono@met.kishou.go.jp

Since 2007, the Japan Meteorological Agency (JMA) has been developing a mesoscale ensemble prediction system (MEPS) using singular vector (SV) methods with the aim of providing probabilistic information for operational mesoscale forecasting (MSM). Recently, the MEPS was upgraded to have an ensemble size of 41 and a horizontal grid spacing of 10 km, assuming a configuration closer to that of the realistic pre-operation system. In addition, some case studies were conducted using this system. These results showed a deficiency of the increasing rate of ensemble spread compared to that of RMSE of the ensemble mean forecast, especially in the latter half of the forecast period in spite of the enhanced ensemble size (Figure 1). One of the reasons is that the uncertainty of the forecast model was not considered in the MEPS. Therefore, development of the stochastic parameterizations for the MEPS has been under way since 2011 to mitigate this deficiency.

In this study, two methods of stochastic parameterization were tested. One is a "random parameter to the Kain-Fritsch (KF) scheme" (RPKF) method and another is a "stochastically perturbed parameterization tendency" (SPPT) method. With RPKF, the sensitivity of the parameters used in the convection scheme (such as trigger function of KF initiation, radius of convective cloud, entrainment coefficient and removing ratio of CAPE) were investigated. The results revealed that only the trigger function showed significant sensitivity to the ensemble spread, and that the effects of the other parameters were small. Accordingly, we only investigate the sensitivity of trigger function in this paper. The random numbers were generated by the normal distribution $N(0, \sigma)$ with a standard deviation σ, and followed the first order Markov process. Spatial correlation was not considered. With SPPT, tendencies from the convection (KF scheme), diffusion and radiation processes were perturbed. Random numbers were also generated by $N(0, \sigma)$ with autocorrelation. Spatial correlation was considered by generating random numbers in the low resolution grid space. The details of the settings are shown in Table 1.

In order to examine the effects of the stochastic perturbations, a case study of ensemble forecasts was investigated in this paper. The MEPS with stochastic parameterizations had a horizontal grid spacing of 10 km and an ensemble size of 11 including control forecast. The initial and lateral boundary values were not perturbed to confirm only the effects of the stochastic parameterizations.

Figure 2 shows the ensemble spread of zonal wind velocity (U) and temperature (T) at 850, 500 hPa and 3 hourly accumulated precipitation (3hRA). The ensemble spread increases until around T+24 except for T at 850 hPa, showing a particular rapid increase in the first three hours. The amplitude of the ensemble spread for SPPT is larger than that for RPKF except with 3hRA, and the ensemble spread of 3hRA for RPKF is larger than that for SPPT in the first half of the forecast period. Figure 3 shows the horizontal distribution of forecasted 3hRA derived from the cloud physics scheme and the KF scheme, and the ensemble spread of each experiment. The spread for RPKF is large in the region where significant amounts of rain are seen from the KF scheme. On the other hand, the ensemble spread for SPPT covers the whole precipitation region. These results reflect that RPKF only perturbs KF precipitation directly via the perturbed trigger function, while SPPT perturbs all precipitation through the KF scheme, radiation and diffusion processes.

Further investigation is needed in regard to the adoption of stochastic perturbation for the MEPS using SV methods with 41 members and a 10-km horizontal resolution. For SPPT, ground variables should be included to perturb the lower atmosphere. In addition, for the random parameter method, other physical processes, such as radiation and diffusion, should also be perturbed, and spatial correlation pattern should be used like SPPT.

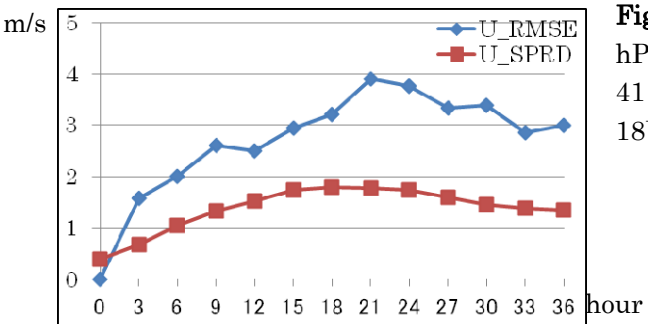

Fig1. Ensemble spread and RMSE of U at 850 hPa from the MEPS with a 10-km grid spacing, 41 members and perturbed by SVs. (initial time: 18UTC on June 10, 2010)

Table1. Details of the stochastic parameterizations.

	RPKF	SPPT
Target	KF trigger function	Tendency of radiation, diffusion and convection
Spatial cor.	None	dx = 500km
Autocorrelation	Markov process, cor.=0.97	e-folding time: 12 hour
σ	1 K	0.2
Limit of perturbation	3 K	0.8

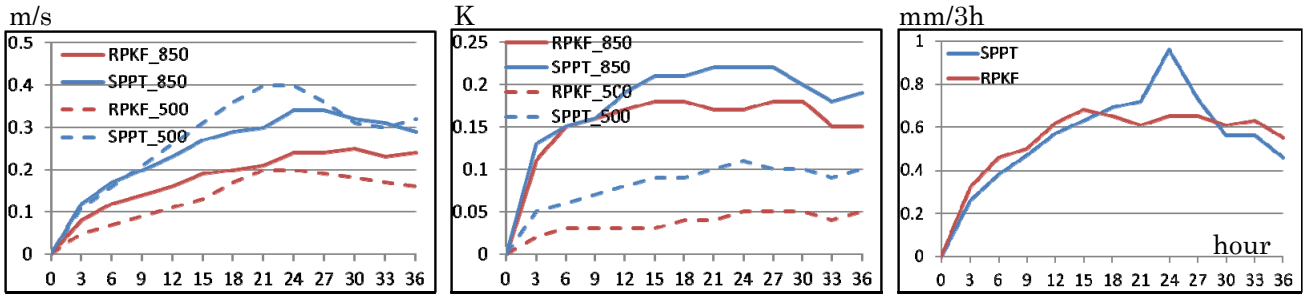

Fig2. Spread of U, T (850, 500) and three-hour accumulated rainfall. (initial time: 18 UTC on June 10, 2010)

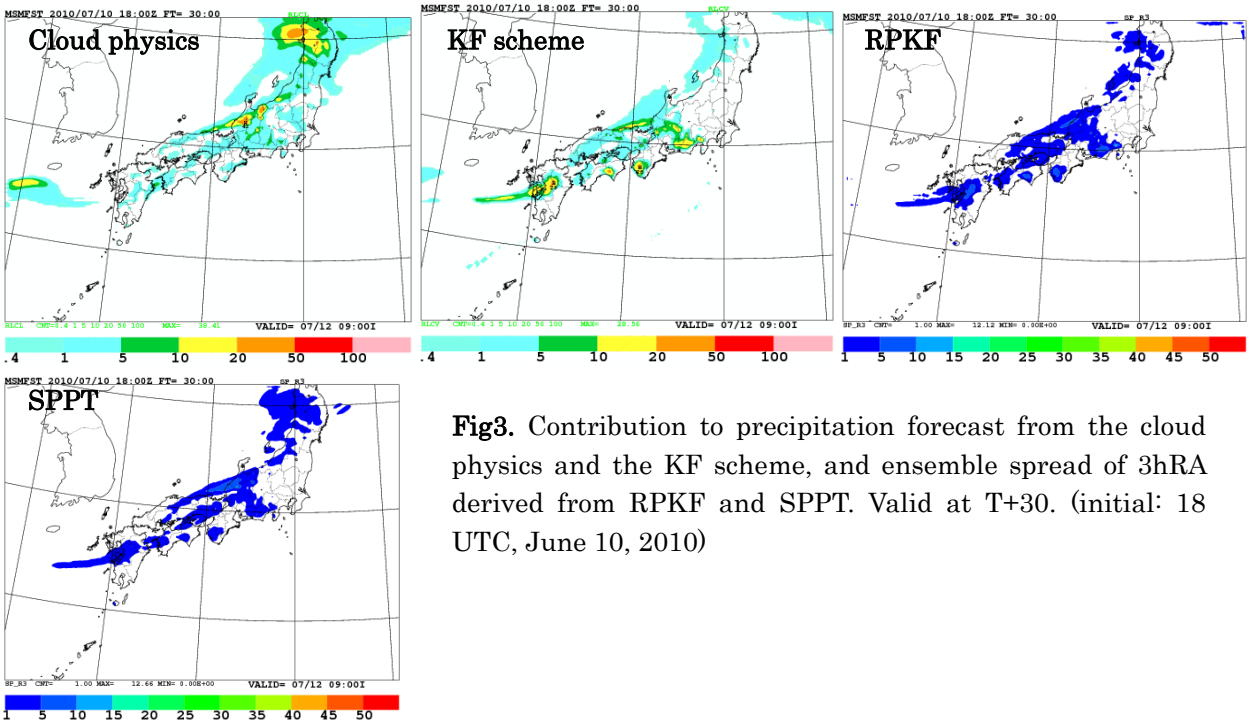

Fig3. Contribution to precipitation forecast from the cloud physics and the KF scheme, and ensemble spread of 3hRA derived from RPKF and SPPT. Valid at T+30. (initial: 18 UTC, June 10, 2010)

CLOUD RESOLVING ENSEMBLE EXPERIMENT OF THE 2011 TYPHOON "TALAS"

Seiji ORIGUCHI[1], Kazuo SAITO[1], Hiromu SEKO[1] and Tohru KURODA[2,1]
[1]Meteorological Research Institute, Tsukuba, Japan
[2]Japan Agency for Marine Science and Technology, Yokohama, Japan

1.Introduction

Typhoon "TALAS", landed in the eastern part of Kochi Prefecture on September 3, 2011, caused local heavy rainfalls over the Kinki, Chugoku, Shikoku and Tokai regions in Japan. It caused enormous landslide disasters in southeastern of Kinki, eastern of Shikoku, Sanin and Tokai, and unprecedented human damages consisting of 78 dead and 16 missing persons. The JMA's operational mesoscale model (MSM) of the days generally well predicted the typhoon track, however, the precipitation intensity was weaker compared with observation. For a socially high impact event, we need to investigate the value of cloud-resolving ensemble forecast.

2.Method of experiment

At first, meso ensemble prediction with a horizontal resolution of 10 km and 11 members was performed up to forecast time (FT) of 36 hr by JMANHM, and its down scaling (cloud resolving ensemble) prediction with a horizontal resolution of 2 km and 11 members was performed up to FT=30. Meso ensemble prediction was conducted using the JNoVA as the initial condition of the control run and the JMA one-week global ensemble prediction as the initial and boundary perturbations. Initial conditions of the 2km ensemble forecast is given by FT=06 of the 10km ensemble forecast result.

3. Results of experiment (verification)

This section shows the results of analysis and verification about 2 km ensemble forecast, where the spin-up period from FT=00 to FT=06 was excluded. Control run (CNTL) track was almost the same that in the best track, but the typhoon speed was faster as in the MSM. Precipitation intensity was closer to the actual data than that of MSM (Fig1(a); circle of broken line). Average of 11 members (MEAN) was weaker than CNTL about the peak of precipitation intensity (Fig1(b); circle of broken line), but the MEAN precipitation areas were broader than CNTL throughout the forecast period. Center position of the typhoon was improved to the south side. Fig1(c) shows the occurrence probability of precipitation intensity over 50mm/3hr. High probability of more than 90% are seen in southeastern of Kinki, eastern of Shikoku, and in Tokai (Fig1(c); circle of broken line). Fig1(d) shows the occurrence probability of precipitation intensity over 100mm/3hr. Probability of more than 35% is seen in southeastern of Kinki, eastern of Shikoku and Sanin (Fig1(d); circle of broken line). Figs.2(a) and 2(b) show the mean error (ME) and the root mean square error (RMSE) of the surface data for the ensemble forecast results at FT=18 against the JNoVA analysis, respectively. MEAN was better than CNTL for wind and sea-level pressure except for temperature and relative humidity (Fig2(a)). MEAN was better than CNTL for all elements (Fig2(b)). About MEs at upper levels, MEAN was better than CNTL for all elements except for wind at 850 and 700hPa and TTD at all levels. About RMSEs, MEAN was better than CNTL about all elements. More detailed verifications are underway according to the four quadrant regions around typhoon (Fig3(g)).

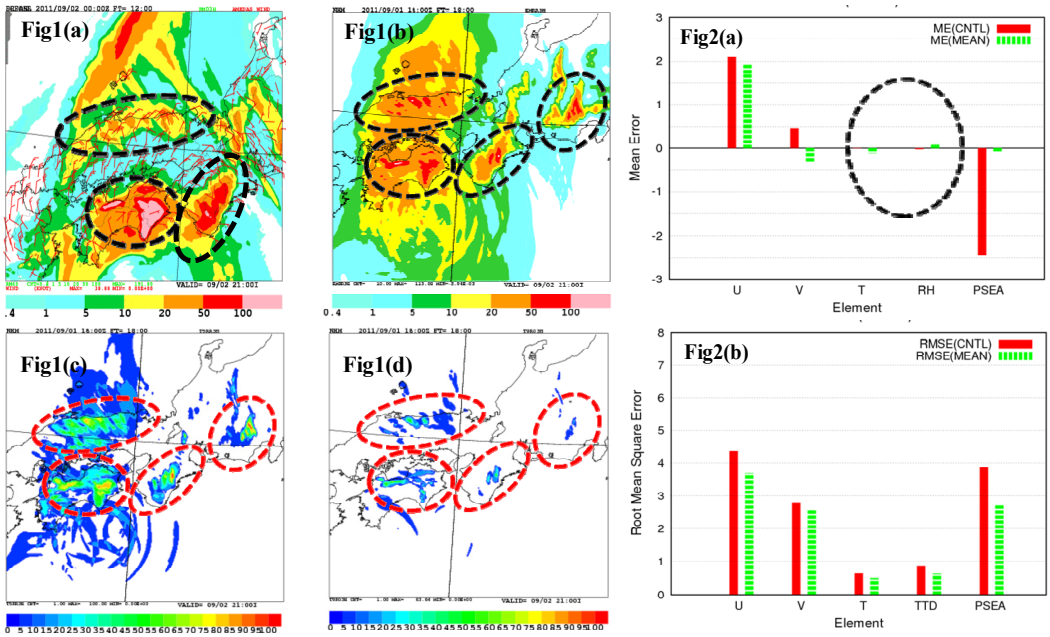

Fig1:(a)Radar-Amedas analysis data(3hr accumulated rainfalls),12UTC Sep2,2011.
(b)Average of 2km-Ensemble forecast (3hr accumulated rainfalls), FT=18.
(c)2km-Ensemble forecast(Occurrence probability of precipitation intensity for 50mm/3hr and more),FT=18.
(d)Same as in (c) but for 100mm/3hr and more.

Fig2:(a)Mean error(Surface) of 2km-Ensemble forecast FT=18 against JNoVA analysis (12UTC Sep2,2011)
(b)Same as in (a) but for Root mean square error(Surface).

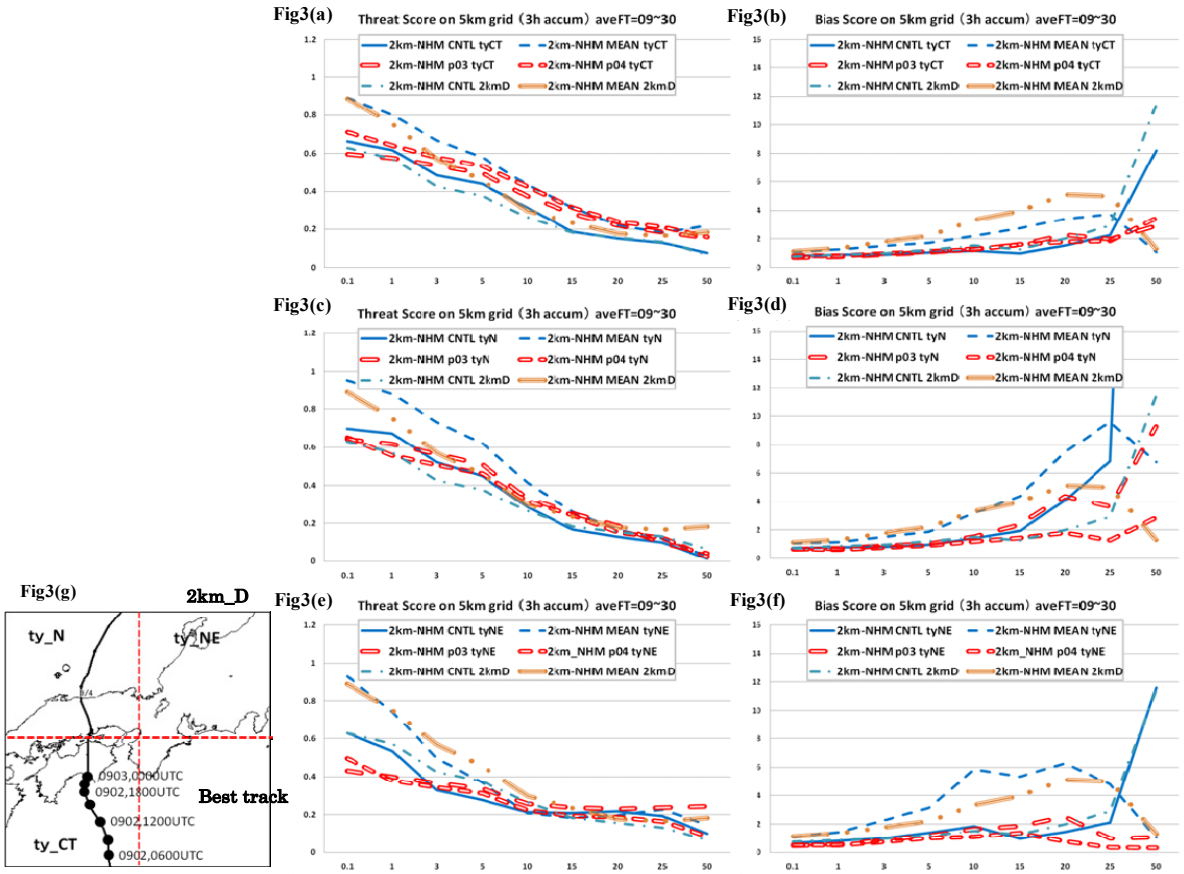

Fig3:Threat Score of 3hr accumulated rainfalls in 2km-Ensemble forecast, average from FT=09 to FT=30 (Left panels). (a)ty_CT and 2km_D. (c)ty_N and 2km_D.(e)ty_NE and 2km_D.
Bias Score of 3 hr accumulated rainfalls in 2 km-Ensemble forecast, average from FT=09 to FT=30 (Right panels). (b)ty_CT and 2km_D. (d)ty_N and 2km_D. (f)ty_NE and 2km_D. (g)Split area and Best track.

Ensemble forecast experiments of 'Yamase' that occurred on 31st July 2011

Hiromu Seko (Meteorological Research Institute), Yasumasa Kodama (Hirosaki University)
and Toshitaka Tsuda (Kyoto University)

1. Introduction

'Yamase' is a cold northeasterly wind that produces cool weather in summer over northeastern Japan. The origin of the Yamase is the cool polar maritime air mass that develops over the North Pacific, including the Bering Sea and the Sea of Okhotsk. It usually accompanies a boundary layer cloud, the "Yamase cloud" (Kodama et al. 2009). 'Yamase' influences the agricultural crops when it continues for long time. It is needed to predict 'Yamase' accurately. In general, 'Yamase' was discussed as a climate problem. However, influences of Yamase can be mitigated by windbreak screens if accurate short range forecasts (1-2 days) are provided. In this study, ensemble forecasts of 'Yamase' were conducted by using the nested LETKF system. The comparisons with the observation data are shown in this report.

2. Outline of experiments

To reproduce the cold northwesterly flow and airflows over the eastern Japan, the nested LETKF system was adopted to the 'Yamase', which occurred from 30th to 31st July 2011. The nested system was composed of two NHM-LETKFs (Miyoshi and Aranami, 2006): Outer and Inner LETKFs. The horizontal grid intervals of Outer and Inner LETKF were 15 km and 1.875 km, respectively. In the Outer LETKF, the conventional data that was used in JMA data assimilation system was assimilated every hour. Although high resolution data, such as Doppler radar data, can be assimilated in the Inner LETKF, the conventional data was assimilated every 10 minutes in this study. Assimilations of the Outer and Inner LETKFs were performed from 09 JST 27th July and 09 JST 31st July, respectively.

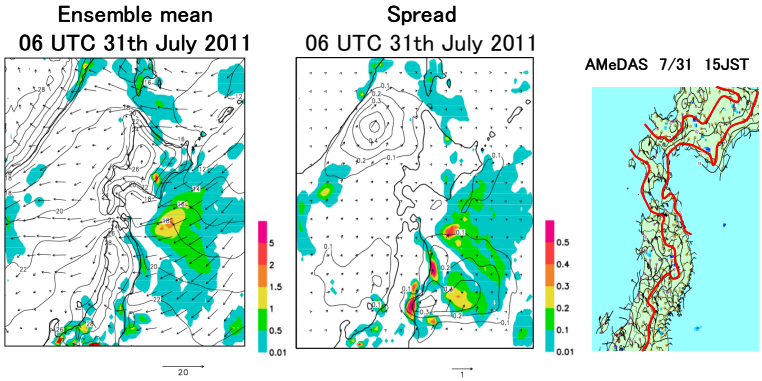

Fig. 1: (left and middle) Ensemble mean and spread at 15 JST 31st July 2011 obtained by Outer LETKF. (right) Temperature and surface wind observed by AMeDAS at 15 JST.

3. Results on ensemble forecasts of Yamase

Figure 1 shows the ensemble mean and spread of sea level temperature, horizontal wind at the height of 20 m and total cloud amount reproduced by the Inner LETKF. On the eastern side of the northern Japan, northeasterly wind was dominant and cold sea level temperature was reproduced. The expanded cloud regions on the eastern side of Japan were also reproduced. The contours of sea level temperature over the northern Japan was roughly similar to the observed ones, which were obtained by Automated Meteorological Data acquisition system (AMeDAS) of JMA, though the reproduced contours were smoother than the observed ones because of the smooth topography of numerical models.

From the water substances of the Outer LETKF, the cloud images were produced. The cloud on the eastern side of the northern Japan was clearly seen in VIS images and obscure in IR images (Fig. 2). These cloud images indicate that this cloud region was composed of low-level stratiform clouds, which is known as the 'Yamase cloud'. There was the relatively fewer region of the cloud along the eastern side of the coastline (Fig. 3). This gap of cloud was reproduced in most of ensemble members.

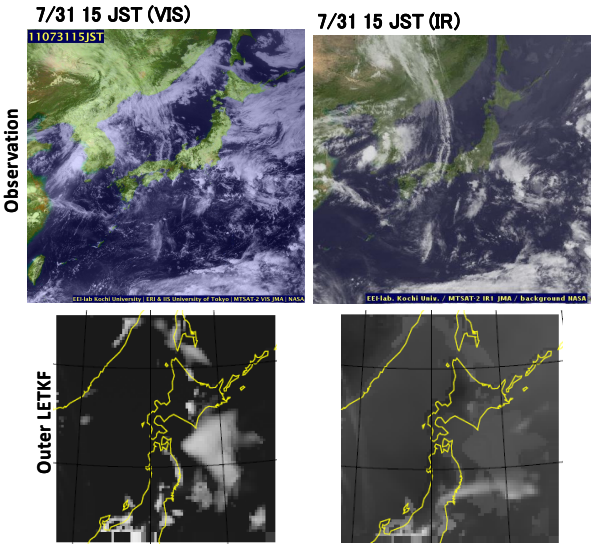

Fig. 2: (upper) Observed satellite images at 15 JST 31st July 2011. (lower) Cloud images produced from outputs of the Outer LETKF.

The temperature and airflow distributions near the surface produced by the Inner LETKF were shown in Fig. 4. As mentioned in the explanation using the analyzed fields of the Outer LETKF, the contours of temperature and surface wind were similar to the observed ones, though the reproduced temperature was slightly colder. The clouds on the eastern side of the mountains and around the eastern coastal line were also consistent with the satellite images. Because these distributions reproduced by the Inner LETKF have small scale structures, the nested LETKF system has the potential to provide the information on temperature and wind speed of 'Yamase' in the inland area of the northern Japan.

The special observation was conducted at the Shimokita peninsula by the Kyoto University and the Hirosaki University (Kodama et al. 2011). In the special observation, sonde, wind profiler and lidar etc. were used to observe the vertical structure of 'Yamase'. When the structure reproduced by the Inner LETKF was compared with the observed ones, the boundary of northerly and southerly winds and the large gradient layers of θe were similar to the observed ones, though the wind speed of the lower layers was weaker.

The vertical structure of 'Yamase cloud' was shown in Fig. 5. 'Yamase cloud' existed at the heights from 1000 m to 1500 m on the eastern side of the northern Japan. The relative humidity below the height of 1500 m exceeded 90 % and temperature of cloud region was colder than the other areas. It is deduced that this cold regions were caused by radiation cooling. The intense northeasterly wind existed mainly below this cloud.

To improve the atmospheric profiles over the sea, the radio occultation data observed by COSMIC was assimilated in the Outer LETKF. Because the refractive index was function of temperature and humidity, the improvements of cloud distribution are expected. Figure 6 shows the distribution of tangent points observed by COSMIC. Even if all COSMIC data in Fig. 6 was assimilated, the improvement of cloud region was not significant (Fig. 3). It is one of reason why the improvement of the cloud regions was small that the positions of COMIS data were far from the cloud regions.

Acknowledgements: The authors would like to express their gratitude to the CDAAC of NCAR, which provided the COSMIC data.

Reference

Miyoshi, T. and K. Aranami, 2006: Applying a four-dimensional local ensemble transform Kalman filter (4D-LETKF) to the JMA nonhydrostatic model (NHM). SOLA, 2, 128-131.

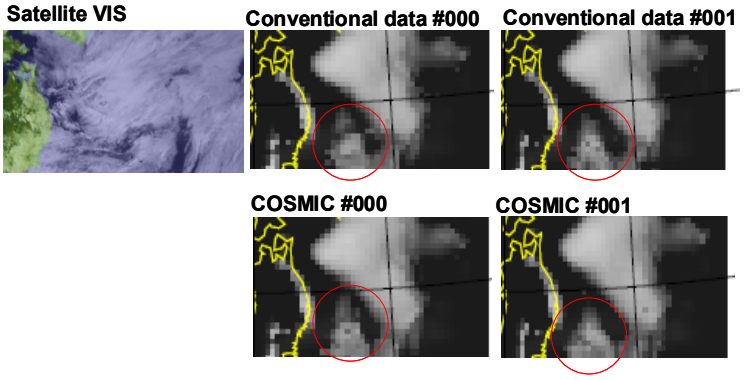

Fig. 3: (left) Observed satellite image (VIS) at 06 UTC. (right) Cloud images obtained from the analyzed fields that were obtained by assimilation of (upper) convectional data and (lower) conventional data and COSMIC data.

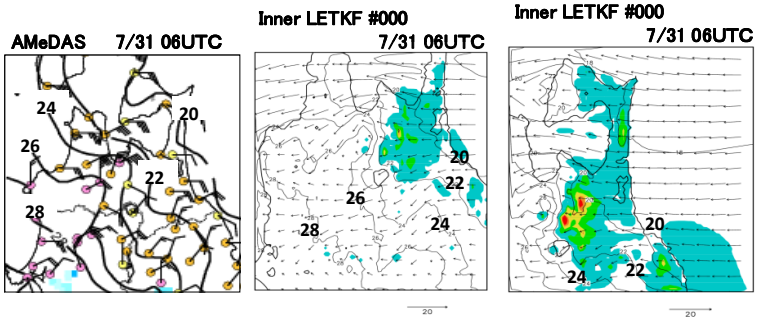

Fig. 4: (left) Temperature and horizontal wind at 15 JST (06 UTC) observed by AMeDAS. (center and right) Temperature and horizontal wind reproduced by the Inner LETKF.

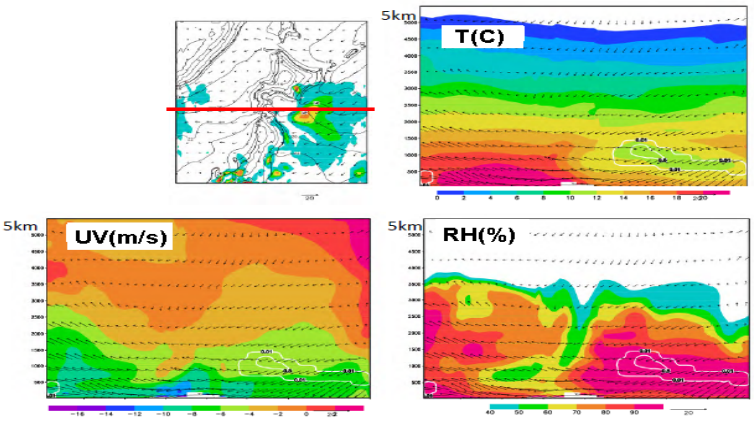

Fig. 5: Vertical cross sections of temperature, wind velocity and relative humidity along a red line.

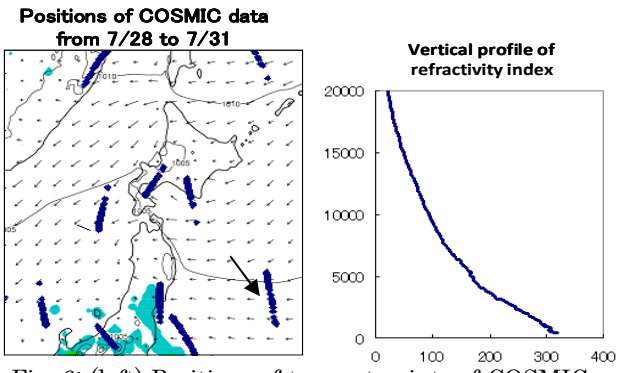

Fig. 6: (left) Positions of tangent points of COSMIC data from 28th to 31st July. (right) Vertical profile of refractivity index. Position of this profile data was indicated by a large arrow.

Ensemble forecast experiments of thunderstorm that occurred in the Kanto Plain on 13th Oct. 2010

Hiromu Seko, Osamu Suzuki, Kazuo Saito (Meteorological Research Institute),
Takemasa Miyoshi (University of Maryland)

1. Introduction

In the last decade, local heavy rainfalls generated in urban areas, such as the Tokyo Metropolitan area, have caused urban flush floods and influenced urban functions (e.g. Zoushigaya local heavy rainfall in 2008). To mitigate the damages from local heavy rainfalls, mechanisms of their developments and movements are needed to be understood. Because local heavy rainfalls are generally generated in mesoscale convergence zones, mesoscale convergences should be reproduced, as well as convection cells. To express mesoscale convergences and convection cells simultaneously, the two-way nested Local Ensemble Transform Kalman Filter (LETKF) system has been developed. In this report, an outline of the nested LETKF system and the assimilation results of the thunderstorm that was developed in the Kanto Plain on 13th October 2010 are explained.

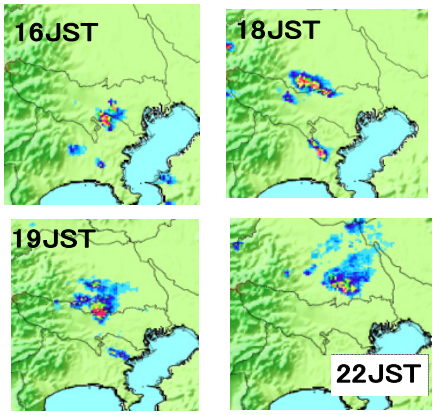

Fig. 1: Rainfall distributions of 13th October 2010 observed by conventional radars of JMA.

2. Thunderstorm developed on 13th Oct. 2010 in the Kanto Plain

Figure 1 shows the rainfall distributions from 16 JST (Japan Standard Time, 9 JST corresponds 0 UTC) by the operational radar of the Japan Meteorological Agency (JMA). New convections that were generated at the southern part of Tokyo by 16 JST moved northward and generated new cells on this northern side. These rainfall regions stayed at the northern part of Tokyo for more than 2 hours. After 21 JST, these rainfall regions moved northeastward and decayed while extending weak rainfall regions northeastward. Figure 2 shows the equivalent potential temperature and sea surface temperature at 20 JST and 23 JST. At 20 JST, the thunderstorm developed at the northern edge of the high equivalent potential temperature airflow from the south. Because the temperature was not much higher than that of the area around the developing point of the thunderstorm, it is deduced that the humid airflow from the south developed it. At 23 JST, a northerly wind region expanded to the south of the rainfall region. Because the moist airflow from the south could not be supplied into the thunderstorm directly, the thunderstorm began to decay. These distributions indicate low-level humid airflow is important for the development and decay of thunderstorms.

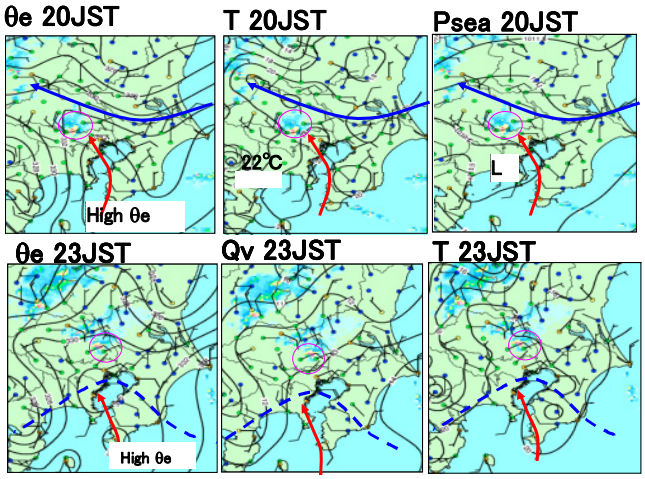

Fig. 2: Surface distributions of equivalent potential temperature, surface temperature, water vapor and sea level pressure at 20 JST and 23 JST13th October 2010.

3. Outline of experiments using the Nested LETKF system

Figure 3 is a schematic illustration of the nested LETLF system. To reproduce mesoscale convergences and convection cells, the nested system was composed of two NHM-LETKFs (Miyoshi and Aranami, 2006): Outer and Inner LETKFs. The horizontal grid intervals of the Outer and Inner LETKFs were 15 km and 1.875 km, respectively. In the Outer LETKF, the conventional data that was used in the JMA data assimilation system was

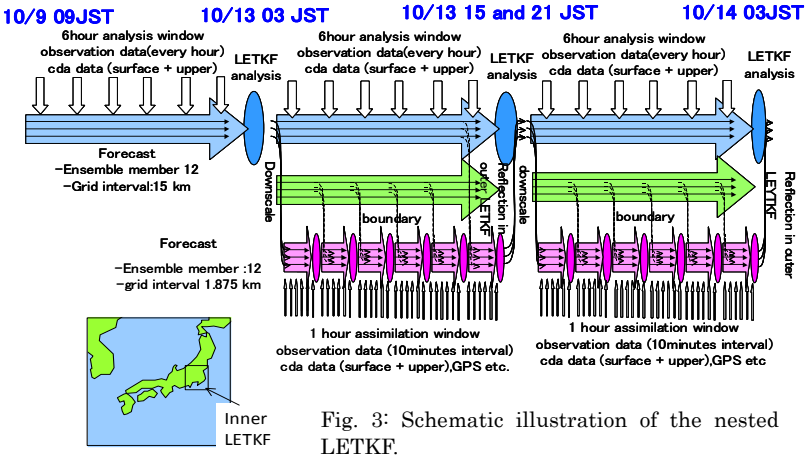

Fig. 3: Schematic illustration of the nested LETKF.

assimilated every hour. The conventional data and GPS-derived PWV data were assimilated every 10 minutes in the Inner LETKF. Assimilations of the Outer and Inner LETKFs were performed from 09 JST 9th October and 03 JST 13th October, respectively.

4. Results of ensemble analyses by the nested LETKF system

Figure 4 shows the ensemble mean and spread of the 1-hour rainfall amount and surface horizontal wind reproduced by the Inner LETKF. Southerly flow from the south converged with easterly flow that covered the northern part of Kanto Plain at 18 JST, and then convection cells **A** were developed at .the convergence area. This convergence area moved northward and other intense convection cells **B** were developed at the northwestern edge of southerly flow. At 24 JST the northerly wind region expanded south of the rainfall region and then the convection cells decayed. This simulated evolution is similar to the observed one, though the position of the reproduced convection cells **B** was shifted northward. However the spread around the convection **B** was too small to correct the position of convection cells **B**. It is deduced that the spread had already become smaller in the Outer LETKF. Other high-resolution data, such as radial wind of Doppler radar is needed to correct the position of convection cells **B**.

In addition to the conventional data, GPS-derived PWV data was assimilated in the Inner LETKF. When PWV data was assimilated, convection cells **A** became more intense and the convection cells **C** were generated near the eastern part of the Kanto Plain (Fig. 5). Because the convection cells **C** was not observed by radars (Fig. 4), PWV data is not sufficient and some other data, such as Doppler radar data, is needed to improve the rainfall forecast of this event.

At 22 JST, a significant vortex was generated near convection cells **B**. Figure 6 shows the mixing ratio of rain and horizontal wind at z=400 m. In three members, significant vortices were generated near the rainfall regions. Although the intensities of the vortices were weak, the vortex near the southwestern tip of the rainfall region was observed by Doppler radar (Fig. 7). The relationship of the rainfall region and vertex reproduced by ensemble member #000 was similar to the observed one. This result indicates the nested LETKF system has the potential to reproduce vortices that may cause tornadoes.

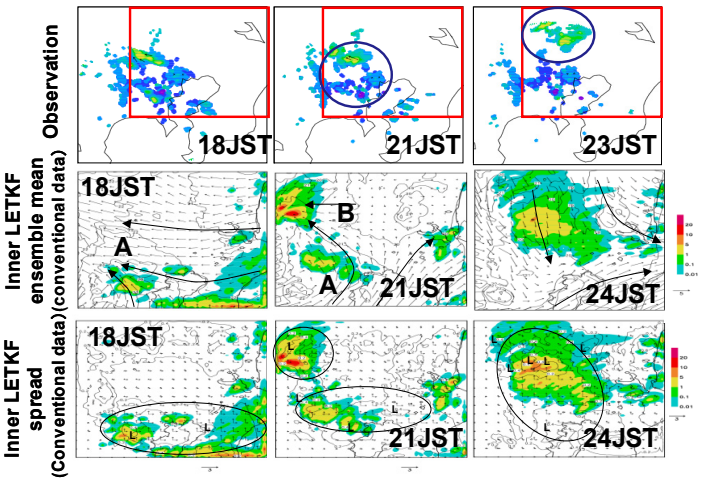

Fig. 4: (upper) Radar echo from 18 JST to 23 JST. (middle) and (lower) Ensemble mean and spread of 1 hour rainfall amount and surface horizontal wind reproduced by Inner LETKF.

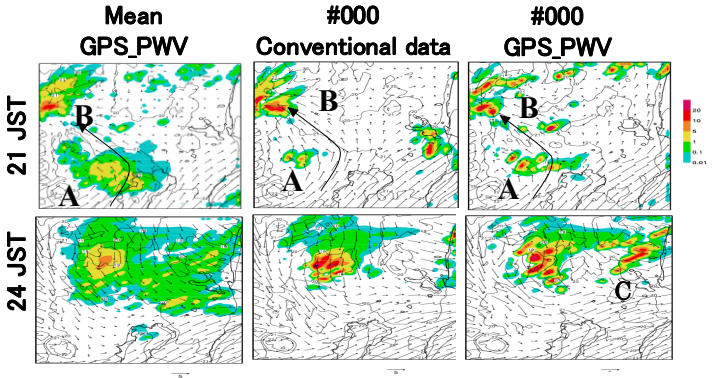

Fig. 5: Ensemble mean and analyses of #000 of 1 hour rainfall amount and surface horizontal wind reproduced by assimilation of convectional data and GPS-PWV data.

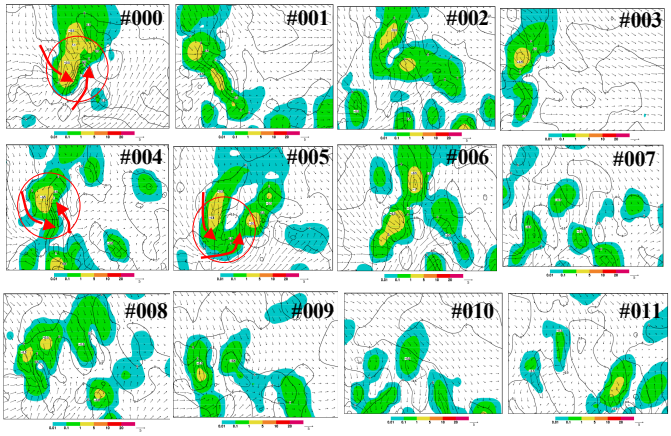

Fig. 6: Mixing ratio of rain at z=20 m and horizontal wind at z=400 m reproduced by assimilation of conventional data.

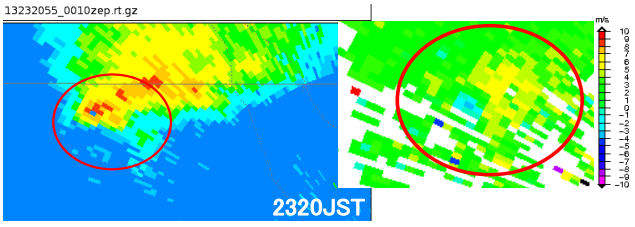

Fig. 7: Radar echo and radial wind at 2320 JST observed by the Tokyo radar..

Acknowledgements

The authors would like to express their gratitude to the Geospatial Information Authority of Japan and Observations Department of JMA, which provided the QZS position data, GPS data and Doppler radar data. The improvements of severe weather forecasts (i.e. local heavy rainfalls), which were achieved by the assimilations of Doppler radars, will contribute to aviation safety and the mitigation of damages of other urban functions.

Reference

Miyoshi, T. and K. Aranami, 2006: Applying a four-dimensional local ensemble transform Kalman filter (4D-LETKF) to the JMA nonhydrostatic model (NHM). SOLA, 2, 128-131.

The predicted quantitative relations between the thermal stratification, wind shear and turbulence parameters

Volf Shnaydman *(Rutgers University, U.S.A.)*
E-mail: volfshn@gmail.com
Leopold Berkovich *(Hydrometeorological Center, Russia)*
Julia Tkacheva *(Hydrometeorological Center, Russia)*

The fields of the wind, temperature, specific humidity and the geopotential on the basic isobaric surfaces, as well as TKE, dissipation rate and turbulence coefficients are predicted in the numerical operational forecasting system of Hydro-meteorological Centre of Russia. The numerical algorithm given in /1/ are used The prediction was carried out for Northern hemisphere using 75km horizontal step and bottom 3-km layer handling the vertical steps of 50m. The initial information is obtained from the objective analysis at 0000UTC 27 June 2010 /2/.

The vertical distribution of meteorological variables and turbulence parameters in two selected points for Moscow (55.8 N, 37.6 E) and Landeck (46.5 N, 10.3 E) which are located in hilly (217m) and mountainous (2444m) areas are represented. The two-day forecasting results given reconstructed the quantitative relations between the thermal stratification, wind shear and turbulence parameters.

The short- term forecasting reconstructed the quantitative relations between the thermal stratification, wind shear and turbulence parameters in the hilly and mountainous areas. At day hours the same meteorological conditions defined the turbulence intensity in both areas. The strong turbulence is predicted from 10m to 1400m with the maximal gradient 60 m^2 / s when the potential temperature gradient was less than –0. 02 deg/100m, and wind module vertical derivatives were small. The strong unstable stratification is a dominant mechanism of the intensive turbulent mixing.In the mountainous area at the nighttime the turbulence is missing when the potential Temperature vertical gradient is more than 0,2 K/100m and the module wind vertical derivative is less than 0.2m/s/100m. The comparison of the meteorological conditions of the turbulence structure in night hours showed that in the mountainous area the turbulence disappeared when the thermal stable stratification is less intensive than in hilly area but the main forcing mechanism remains the influence of stable stratification.In the hilly area the turbulence missing at the nighttime when the potential temperature vertical gradient is more than 0,5 K/100m and the module wind vertical one is less than 0.2m/s/100m. But above the strong stable stratified lowest layer of the 500m height the turbulence coefficient is more than 1 m^2 / s in the layer from 500m to 1500m with the maximum of 4 m^2 / s -23 m^2 / s on 700-800m when potential temperature

vertical gradient is less 0.5 K /100m and the wind module derivative is more than 1m/s/100m.

The large-eddy simulation studies showed that during late afternoon and early morning (the transition periods) the decoupled residual layer, where turbulence is still active, developed above the stably stratified lower part of boundary layer /3/. In a concerted effort to learn more, the project is gathering the scientists from the European Union and the United States to work on this issue and to make observations for better understanding the physical processes that control the role of this transition in the turbulence structure /4/.

This study reveals the transition time of the turbulence activity development. It confirms the existence of residual turbulent layers and gives the quantities description of meteorological variables and turbulence parameters in these layers.

The results obtained allowed to estimate the horizontal distribution of the turbulence parameters. As an example the maximal vertical coefficients represented the turbulence strength at 1200UTC of 27/06 and 28/06 are given below for different latitudes and longitudes.

65-61N 1- 55 m^2/s^2, 0-42E.

61-56N 5-25 m^2/s^2, 0-8E 26 m^2/s^2 -55 m^2/s^2, 9-42E.

56-51N 30 m^2/s^2 - 5 m^2/s^2, 0-25E, 6 m^2/s^2 - 47 m^2/s^2, 26-42E.

51-46N, 18-35 m^2/s^2, 0-22E, 36 -56 m^2/s^2, 23-42E.

46-42N, 21-45 m^2/s^2, 0-18E, 46-57 m^2/s^2, 19-42E.

65-61N, less than 1 m^2/s^2, 0-10E, 1-65 m^2/s^2, 11-42 E.

61-56N, 45 m^2/s^2 -25 m^2/s^2 ,0-8 E, 26 m^2/s^2 -55 m^2/s^2. 9-42 E.

56-51N, 30 m^2/s^2 -5 m^2/s^2, 0-25 E, 6 m^2/s^2 -47 m^2/s^2, 26-42 E.

51-46N, less than 1 m^2/s^2, 0-11 E, 1-33 m^2/s^2, 12-22 E, 32-8 m^2/s^2, 23-32 E, 9 m^2/s^2 -34 m^2/s^2, 33-42 E.

46-42N, 30-1 m^2/s^2, 0-10 E, 2-53 m^2/s^2, 12-36 E, 52-28 m^2/s^2, 37-42 E.

At the noon the maximal turbulence coefficient had the large diversity. Its values got 65 m^2/s^2. At the night the turbulence is missing in the most points of calculation net. But the turbulence coefficients got 5-10 m^2/s^2 in the points where the predicted coefficients in noon were more than 50 m^2/s^2. It's related with the existence of the residual above the strong stable stratification.

1.Shnaydman V. (2010) Improved numerical solution of three-dimensional turbulence closure equations. Research Activity in Atmospheric and Oceanic Modeling #40, 4-13

2. Shnaydman V.,Berkovich L.,Tkacheva Ju. (2011) Forecast of Meteorological Variables and Turbulence Parameters. Research Activity in Atmospheric and Oceanic Modeling #41, 5-21

3.Pino D, Jonker J, Vilà-Guerau de Arellano, Dosio A (2006), Role of shear and the inversion strength during sunset turbulence over land: Characteristic length scales. Boundary Layer Meteorol., 121: 537–556

4.Lothon M, Lenschow D (2010) Studying the Afternoon Transition of the Planetary Boundary Layer. EOS (American Geophysical Union) vol. 91, # 29